JOURNAL OF GEOPHYSICAL RESEARCH, VOL. 103, NO. D5, PAGES 5797–5814, MARCH 20, 1998

Modeling ozone laminae in ground-based Arctic wintertime observations using trajectory calculations and satellite data

G. L. Manney,[1] J. C. Bird,[2] D. P. Donovan,[2] T. J. Duck,[3] J. A. Whiteway,[4]
S. R. Pal,[2,3] and A. I. Carswell[2,3]

Abstract. Reverse-trajectory calculations initialized with ozone observed by the Upper Atmosphere Research Satellite Microwave Limb Sounder (MLS) provide high-resolution ozone profiles for comparison with lidar and ozonesonde observations from the Arctic Stratospheric Observatory facility near Eureka in the Canadian Arctic (~80°N, 86°W). By statistical measures, calculated profiles show a small average improvement over MLS profiles in the agreement of small-scale structure with that in ground-based observations throughout the stratosphere, and a larger (although still modest) and more consistent improvement in the lower stratosphere. Nearly all of the calculated profiles initialized with daily gridded MLS data show some improvement in the lower stratosphere. Even in cases where overall agreement between profiles is mediocre, there are frequently one or more individual features in the calculated profiles that strongly resemble laminae in the ground-based observations. Differential advection of ozone by the large-scale winds leads to lamination in three distinct ways. Filamentation results in lamination throughout the stratosphere, with comparable features arising from initializations with gridded MLS data and with potential vorticity/θ-space reconstructions of MLS data (reconstructed (RC) fields). Laminae also form in the middle and lower stratosphere in conjunction with intrusions into the vortex; while calculations initialized with RC fields produce laminae, the agreement of structure calculated using gridded MLS initialization data with ground-based observations is distinctly better. Inside the lower stratospheric vortex, laminae form by advection of local features in the MLS initialization fields; RC-initialized calculations fail to produce any significant features since these local ozone variations are not strongly correlated with potential vorticity. That local features observed by MLS are needed to produce laminae resembling those in independent ground-based observations at Eureka indicates that both datasets are capturing real atmospheric features.

1. Introduction

Small vertical scale structures, or laminae, in stratospheric ozone profiles have been observed for many years [e.g., *Reid and Vaughan,* 1991, and references therein]. *Reid and Vaughan* [1991] found that ozone laminae were most common in winter and spring near the polar vortex edge in the lower stratosphere, and several studies suggest that laminae in this domain result from differential advection of ozone by the large-scale winds. Modeling studies show differential advection leading to the formation of narrow filaments of material pulled off the vortex and intrusions into the vortex in the lower stratosphere [e.g., *Waugh et al.,* 1994; *Plumb et al.,* 1994]; other studies show small horizontal scale structures along the vortex edge and in the anticyclone throughout the stratosphere [e.g., *Pierce and Fairlie,* 1993; *Sutton et al.,* 1994]. *Orsolini* [1995] and *Schoeberl and Newman* [1995] demonstrated how small horizontal scale structures such as these which tilt with height may lead to lamination in idealized tracers. *Orsolini et al.* [1997] used ozone from the Upper Atmosphere Research Satellite (UARS) Microwave Limb Sounder (MLS) to initialize high-resolution transport calculations and demonstrated that advection by the large-scale wind field gave rise to small vertical scale structures resembling those observed in a lidar ozone profile in the lower stratosphere through the process of filamentation.

The Arctic Stratospheric Observatory (AStrO) near Eureka, Canada (80.05°N, 86.42°W), has, since early February 1993, provided high vertical resolution ozone profiles from both differential absorption lidar (DIAL) and ozonesondes [e.g., *Donovan et al.,* 1995]. Because of the location of AStrO and the variability of the Arctic polar vortex, these observations sample a variety of conditions both inside and outside the vortex over the course of a winter. As described by

[1]Jet Propulsion Laboratory/California Institute of Technology, Pasadena, California.
[2]Center for Research in Earth and Space Technology, North York, Ontario, Canada.
[3]Department of Physics and Astronomy, York University, North York, Ontario, Canada.
[4]Department of Physics, University of Wales, Aberystwyth, Wales, United Kingdom.

Paper number 97JD03449.
0148-0227/98/97JD-03449$09.00

Bird et al. [1997], ozone laminae with a variety of vertical scales have been observed over Eureka throughout the stratosphere; this is consistent with the theoretical study by *Appenzeller and Holton* [1997] which showed that tracer lamination resulting from differential advection by a vertically sheared wind field is expected at all levels along the edge of the winter polar vortex. Calculations using an idealized tracer field suggest that some of the structures observed at AStrO may originate through filamentation driven by differential advection by the large-scale wind field [*Bird et al.*, 1997].

We have identified lidar and ozonesonde profiles from AStrO with laminated structures that were observed at times when UARS MLS provided three-dimensional (3-D) ozone data (albeit with low horizontal and vertical resolution) 6–15 days prior to the ground-based measurements. These MLS data are used to initialize calculations of high-resolution ozone profiles for comparison with the ground-based observations. The ability of these calculations to produce features resembling those in ground-based observations and the mechanisms by which laminae form in the calculations are studied, both to explore the origins of ozone laminae in and around the Arctic polar vortex and to examine the consistency between MLS and ground-based ozone observations.

2. Data and Analysis

2.1. Ozone Data From AStrO

Ozone measurements are carried out using a XeCl excimer DIAL system utilizing 308 nm as the "on" wavelength and hydrogen stimulated Raman shifted 353 nm as the "off" wavelength. The details of the system are described by *Carswell et al.* [1991]; it has since been modified to include nitrogen Raman returns at 332 and 385 nm corresponding to the 308 and 353 nm wavelengths, respectively. The profiles shown here represent the "nightly mean" ozone, an average over several hours. The vertical resolution of these profiles is typically ~300 m. The nightly mean ozone concentration statistical uncertainty is typically better than 5% up to ~40 km [*Steinbrecht*, 1994]. Exceptions to this are when the observing period was much shorter; in such cases, uncertainties become large in the middle and upper stratosphere. In 1993, lidar measurements in the lower stratosphere were affected by the high aerosol loading resulting from the eruption of Mount Pinatubo [*Steinbrecht and Carswell*, 1995]; this typically affected measurements below ~18 km, but at times when the vortex was shifted well away from AStrO so that midlatitude air was observed, this problem extended up to ~22 km.

Ozone profiles from ground level to ~35 km altitude are obtained from electrochemical concentration cell (ECC) ozonesondes that are launched about three times a week from Eureka (~10 km SE of the AStrO facility). These profiles have a vertical resolution near 400 m for measurements taken before the beginning of the 1994-1995 season and near 40 m for subsequent measurements. The balloon flights typically last 2-3 hours, and the sonde position may drift from over Eureka by several hundred kilometers, depending on the wind conditions. The ECC ozonesonde observations typically have precision and accuracy of ~6% and ~10%, respectively [*McDermid et al.*, 1990]. Comparisons between lidar and ozonesonde observations at AStrO indicate good agreement within the uncertainties of the observations [*Donovan et al.*, 1995].

2.2. Ozone Data From MLS

The MLS ozone data are version 4 retrievals from the 205 GHz radiometer; they have a horizontal resolution of ~400 km and are retrieved on a vertical grid with ~5-km spacing [*Froidevaux et al.*, 1996]. The MLS version 3 ozone data and validation are described in detail by *Froidevaux et al.* [1996]. Version 4 changes include retrieval of nitric acid in the same band as ozone [*Santee et al.*, 1996] and refinements in tangent pressure retrievals, field-of-view pointing, and estimated errors. Precisions (rms) of individual ozone measurements from 50 to 1 hPa are ~0.2-0.3 parts per million by volume (ppmv), with absolute accuracies of ~5%-10% in the middle and upper stratosphere, and 10%-20% in the lower stratosphere [*Froidevaux et al.*, 1996]. The reliability of the MLS ozone data at 100 hPa is more variable, and absolute accuracy can range from 25% to >50% (especially at low latitudes), but more sensitivity is achieved in version 4 than in version 3 data.

The UARS platform orientation causes the MLS instrument to switch between viewing ~34°S to 80°N and ~80°S to 34°N approximately every 36 days [e.g., *Reber*, 1993]. This provides coverage of high northern latitudes through December and February, with early winter observations beginning in middle or late November, and late winter observations extending to early or middle March, depending on the year. The MLS scan mechanism began to show signs of wear in late 1993, and the UARS spacecraft has been operating with reduced power since mid-1995, resulting in periods of missing data and less than daily frequency of MLS observations during the last four Arctic winters.

When MLS data were available for periods of weeks with no gaps longer than 1-2 days, a Fourier transform technique that separates time and longitude variations [*Elson and Froidevaux*, 1993] was used to grid the data (referred to here as "asynoptic mapping"); this procedure is most valuable when the data are available daily with no data gaps. In addition, a cruder gridding procedure (referred to as "simple gridding") consists of binning all data taken over a 24-hour period in latitude/longitude bins and assigning to the appropriate gridpoint a weighted average of the values that fall within the bin; the main advantage of this is that only one day of data is needed. Comparisons generally show differences between the two procedures to be small. For most of the cases shown here both methods can and have been used with comparable results.

2.3. Transport Calculations

High-resolution ozone profiles and maps are generated from the MLS observations using a variation of the reverse-

trajectory technique developed by *Sutton et al.* [1994]. The horizontal winds used are from the United Kingdom Meteorological Office (UKMO) data assimilation system [*Swinbank and O'Neill,* 1994]. The trajectory code [*Manney et al.,* 1994] uses a standard fourth-order Runge-Kutta scheme, with once-daily winds (and temperatures for 3-D calculations) that are linearly interpolated to the trajectory time step ($^1/_2$ hour) and to the starting times of the calculations. Both isentropic and 3-D trajectory calculations were done for each profile; the 3-D calculations use UKMO temperatures and a middle atmosphere radiation code to obtain vertical velocities in isentropic coordinates. The trajectory code and its implementation using UKMO data are described in detail by *Manney et al.* [1994].

The reverse-trajectory technique [*Sutton et al.,* 1994] involves trajectory calculations for parcels initially located at the positions and times at which the final high-resolution field is desired. A back-trajectory calculation is run for the ensemble of parcels to a time for which the initialization data (in this case, MLS ozone) are available. These data are interpolated to the parcel positions. Since it is assumed that ozone is passively transported, the ozone mixing ratio at the original locations of the parcels will simply be equal to this interpolated value. Thus the tracer field is effectively advected forward in time, although the trajectory calculation is done backward. As discussed by *Sutton et al.* [1994] and *Schoeberl and Newman* [1995], the resolution of the final field depends both on the spacing of the parcel grid (this is the best resolution that can be obtained) and the length of the back trajectory calculation (as smaller-scale features develop for longer calculations). *Sutton et al.* [1994] discuss the implications of development of small scales and nonconservative processes on the selection of the length of runs in some detail.

Sutton et al. [1994] initialized parcels on a dense horizontal grid and did isentropic trajectory calculations to obtain high-resolution maps of passive tracer mixing ratios. In addition to this, *Schoeberl and Newman* [1995] and *Newman and Schoeberl* [1995] initialized parcels on dense θ-latitude and/or θ-longitude sections to obtain high-resolution fields of idealized tracers showing vertical structure. Here we obtain high vertical resolution profiles by initializing parcels in a column centered over AStrO. The parcels are placed on 100 isentropic surfaces, equally spaced in $\log(\theta)$, between 400 and 1400 K (~100-3 hPa); this corresponds to a vertical spacing (and therefore a best vertical resolution) of ~250-280 m, comparable to the resolution of the lidar data. To obtain information about the sensitivity of the calculations to the exact initial parcel positions, an 11 by 11 array of parcels is placed in a 2° longitude by 0.5° latitude (~50 km square) box centered over AStrO. The differences between high-resolution ozone profiles obtained from individual and average parcel results help in assessing the reliability of the calculations.

Since the lidar profiles represent an average over several hours, the trajectory calculations are initialized at approximately the middle of the measurement period; calculations being matched to ozonesonde profiles are initialized in the middle of the time period for which the balloon's potential temperature was between 400 and 700 K, typically about $1\ ^1/_2$ hours into the flight. The back-trajectory calculations for most cases were run for 11–12 days (depending on the time of day of the ground-based observation), with the results saved once daily at 1200 UT (the time for which UKMO and gridded MLS data are available), so simulated profiles can be compared for varying calculation times. Statistical analyses like those discussed in sections 2.5 and 3.1 showed comparable results for calculations from 7 to 12 days length with overall better agreement with the data we are trying to model than for shorter runs. The availability of MLS data for initialization is such that 11–12 day calculations can be done for more cases than 7–8 or 9–10 day lengths; hence detailed results are shown for calculations of that length.

High-resolution ozone maps were made on selected isentropic surfaces (with θ values selected from the set of 100 levels on which the profiles were generated) using the same reverse-trajectory procedure. Parcels were placed on an equal area grid from 40° to 90°N with 0.5° latitude spacing and 0.5° longitude spacing at the equator (~50 by 50 km spacing). The resulting high-resolution fields are interpolated to a 0.5° latitude by 1.8° longitude grid for plotting. For computational efficiency most of these maps were produced using isentropic trajectory calculations.

2.4. Initialization Fields

Initialization fields are obtained from MLS data in several ways. In addition to the asynoptically mapped (AM) (when feasible) and simply gridded (SG) MLS ozone fields, a third set of low-resolution data (reconstructed (RC) data) was used. Ozone fields were reconstructed from MLS ozone mapped into potential vorticity (PV)/θ space [e.g., *Schoeberl et al.,* 1989]. An average ozone field as a function of PV (calculated from UKMO data) and θ was constructed using ozone and PV from 3–5 days near the initialization time. A field in geographical space for an individual day was then reconstructed using PV for that day. The ozone fields resulting from this procedure are very smooth but maintain the general large-scale vertical and horizontal gradients present in the MLS ozone. By comparing the resulting high-resolution profiles to those initialized using individual days of MLS data, we can study when and if specific local features in the MLS data are important to producing small vertical scale structures resembling those in ground-based ozone observations. When necessary, values at latitudes higher than those observed by MLS are filled in by interpolation across the pole for AM and SG initializations. The calculated profiles analyzed in detail result from initialization with data from regions covered by actual MLS observations at all or nearly all levels.

2.5. Statistical Analysis

To quantify the ability of the transport calculations to produce realistic small scale structure in ozone profiles, several statistical comparisons were done, including RMS dif-

ferences, correlation coefficients (and their significance levels according to a Student's t-test), and the Kolmogorov-Smirnov (KS) significance [e.g., *Gibbons,* 1985]. Our approach follows *Fairlie et al.* [1997] and *Pierce et al.* [1997]. For each observed profile we have calculated the "expected" KS significance using a Monte Carlo simulation by calculating the KS significance between the observed lidar or ozonesonde profile and the observed profile plus a randomly distributed 10% rms error for 200 such simulated profiles. The average KS significance and its standard deviation resulting from this procedure give a measure of the sensitivity of the KS significance for each profile to imposed errors and aid in the interpretation of the KS significance values between the observed and calculated profiles. For comparisons requiring data on the same vertical grid we have interpolated the ground-based and MLS observations linearly in $\log(\theta)$ to the model grid. The KS significance between the interpolated and uninterpolated observations is very high ($\gtrsim$0.99), indicating that this interpolation has not introduced significant biases.

Correlation coefficients and rms differences are strongly affected by even slight differences in the altitude of features being compared. As discussed by *Fairlie et al.* [1997], the KS test is useful because, since it compares frequency distributions, altitude differences do not affect it. One could, in fact, construct profiles with similar features offset by many kilometers which had identical frequency distributions. Calculating rms differences and correlation coefficients for profiles that are first shifted in the vertical by small increments (the largest shift being no more than 3 km) provides additional information on the general resemblance between profiles when a small offset in their altitudes is taken into account.

To examine the agreement between profiles with and without large-scale biases, we show statistical calculations for the raw profiles and for profiles with a third-order polynomial fit removed (referred to as "Δ3P profiles"). The statistical comparisons are done for the entire profile (from 400 to either 1400 K (the top level of the transport calculations) or the highest level in the ozonesonde observations), for the lower stratosphere (400–655 K), and for the middle stratosphere (664–1087 K). The polynomial fits are calculated only over the region being compared. Since the ozonesonde data extend to only ~30 km (~850 K), "middle stratosphere" statistics are not calculated for them. For each type of initialization field (AM, SG, and RC), the statistical calculations were done for both 3-D and isentropic calculated profiles and for the profiles calculated from both the individual parcels at each level centered over AStrO and from the average of 121 parcels at each level. All 42 ground-based observations, comprising 30 lidar and 12 ozonesonde profiles, can be compared using the RC initialization; 25 (20 lidar and 5 ozonesonde) can be compared using the AM initialization; and 28 (21 lidar and 7 ozonesonde) can be compared using the SG initialization.

2.6. Other Considerations

UKMO temperatures were used to interpolate gridded MLS ozone to isentropic surfaces. The ground-based observations also have temperatures associated with them. To check whether interpolating the ground-based profiles to isentropic surfaces using these temperature profiles versus UKMO temperatures introduced a bias, we have also calculated the potential temperature values for the ground-based observations from UKMO temperatures and compared the profiles thus obtained as a function of θ with those obtained using temperatures from the ground-based observations. Of all the profiles studied, there was only one for which there was a discernible difference, consisting of a slight shift in the altitude of features in the profile.

The periods examined comprise middle February to middle March 1993, December 1993 to early January 1994, February to middle March 1994, February to early March 1995, December 1995, February to early March 1996, December 1996, and February 1997. Although we discuss results for the middle stratosphere, our primary focus is on the lower stratosphere (~400-700 K), where in absence of heterogeneous processing on polar stratospheric clouds the lifetime of ozone is long compared to the timescale of dynamical variations [e.g., *Brasseur and Solomon,* 1986]. It has been shown that chemical ozone loss occurred in the Arctic lower stratosphere during some of these periods. This may affect our results for cases during these periods for which we examine profiles observed within the Arctic vortex.

3. Results

3.1. Average Statistical Results

Table 1 summarizes the key average results of the statistical calculations for the raw and Δ3P (third-order polynomial fit removed) profiles. Average correlation coefficients and KS significance and their standard deviations are shown for the calculated profiles constructed from the average of 121 parcels at each level; results for the central profiles are nearly identical. Except for three profiles for which MLS data were available only 6–8 days prior to the ground-based observations, the results shown here are from runs of 11–12 days length.

All correlation coefficients for the raw (no polynomial fit removed) profiles are significant at the 95% confidence level (c.l.) for the lower stratosphere and for the entire profiles, indicating general agreement between the overall structure of the profiles. The slight decrease in the correlation coefficient between the raw calculated and ground-based profiles over that between the raw MLS and ground-based profiles seen in Table 1 indicates that the transport calculations do not reduce overall biases between MLS and ground-based observations. However, the correlation coefficients for the Δ3P profiles are a much more sensitive measure of the agreement between the small-scale structure in the profiles. The correlation coefficients for calculated versus MLS Δ3P profiles also decrease when the comparisons are done over the entire depth of the profile, indicating that by this measure the calculations do not even improve the overall agreement of smaller-scale structure (over the entire depth), much less any large-scale biases. The increase in the correlation coefficients for calculated and ground-based Δ3P profiles over those for MLS and

Table 1. Summary of Statistical Calculations.

Profile Type	Raw Profiles: Correlation Coefficient	KS Significance	#KS > Expected	%KS Improved	Third-Order Polynomial Removed: Correlation Coefficient	KS Significance	#KS > Expected	%KS Improved
			Entire Profile (400–1400 K)					
SG (28 Profiles)								
MLS	0.82 ± 0.20	0.05 ± 0.15	1		0.26 ± 0.36	0.01 ± 0.01	0	
ISN	0.81 ± 0.17	0.04 ± 0.10	0	46%	0.20 ± 0.27	0.09 ± 0.16	4	86%
3-D	0.78 ± 0.22	0.08 ± 0.17	1	50%	0.19 ± 0.28	0.12 ± 0.17	4	93%
AM (25 Profiles)								
MLS	0.82 ± 0.20	0.04 ± 0.08	0		0.24 ± 0.31	0.02 ± 0.04	1	
ISN	0.80 ± 0.17	0.03 ± 0.09	0	32%	0.14 ± 0.25	0.08 ± 0.13	4	92%
3-D	0.77 ± 0.23	0.08 ± 0.15	1	40%	0.14 ± 0.30	0.15 ± 0.23	4	92%
RC (41 Profiles)								
MLS	0.79 ± 0.25	0.08 ± 0.18	0		0.22 ± 0.29	0.04 ± 0.11	2	
ISN	0.79 ± 0.25	0.09 ± 0.17	1	46%	0.18 ± 0.31	0.08 ± 0.19	5	63%
3-D	0.76 ± 0.27	0.10 ± 0.17	1	51%	0.17 ± 0.31	0.11 ± 0.18	6	78%
			Lower Stratosphere (400–654 K)					
SG (28 Profiles)								
MLS	0.95 ± 0.07	0.28 ± 0.26	0		0.02 ± 0.46	0.01 ± 0.03	2	
ISN	0.94 ± 0.05	0.30 ± 0.28	1	57%	0.18 ± 0.35	0.39 ± 0.33	13	100%
3-D	0.95 ± 0.05	0.36 ± 0.32	2	57%	0.22 ± 0.35	0.42 ± 0.35	15	96%
AM (25 Profiles)								
MLS	0.96 ± 0.04	0.32 ± 0.30	0		0.03 ± 0.47	0.05 ± 0.15	4	
ISN	0.95 ± 0.03	0.32 ± 0.26	1	32%	0.16 ± 0.36	0.40 ± 0.31	15	96%
3-D	0.95 ± 0.02	0.34 ± 0.31	1	36%	0.21 ± 0.35	0.41 ± 0.33	12	92%
RC (42 Profiles)								
MLS	0.95 ± 0.05	0.40 ± 0.30	3		0.21 ± 0.42	0.02 ± 0.05	1	
ISN	0.95 ± 0.05	0.37 ± 0.29	3	31%	0.27 ± 0.37	0.23 ± 0.29	13	79%
3-D	0.95 ± 0.04	0.40 ± 0.32	6	45%	0.29 ± 0.37	0.22 ± 0.27	13	83%
			Middle Stratosphere (665–1087 K)					
SG (21 Profiles)								
MLS	0.43 ± 0.43	0.04 ± 0.07	1		0.29 ± 0.30	0.03 ± 0.06	0	
ISN	0.36 ± 0.37	0.07 ± 0.17	1	52%	0.26 ± 0.33	0.28 ± 0.32	7	86%
3-D	0.41 ± 0.34	0.06 ± 0.11	0	52%	0.32 ± 0.26	0.33 ± 0.32	10	95%
AM (20 Profiles)								
MLS	0.43 ± 0.41	0.02 ± 0.04	0		0.29 ± 0.31	0.08 ± 0.16	3	
ISN	0.32 ± 0.36	0.11 ± 0.23	2	65%	0.20 ± 0.36	0.25 ± 0.30	6	80%
3-D	0.38 ± 0.36	0.05 ± 0.10	0	50%	0.28 ± 0.30	0.35 ± 0.31	10	90%
RC (30 Profiles)								
MLS	0.37 ± 0.44	0.13 ± 0.21	0		0.06 ± 0.44	0.07 ± 0.20	2	
ISN	0.36 ± 0.43	0.10 ± 0.19	1	40%	0.04 ± 0.39	0.20 ± 0.25	9	77%
3-D	0.36 ± 0.36	0.05 ± 0.09	0	27%	0.08 ± 0.40	0.26 ± 0.28	10	83%

Values presented are for profiles calculated from the average of 121 parcels at each level compared to the ground-based observations. Parenthesized numbers following the initialization type (SG, AM, and RC) indicate the number of profiles included in the average. The abbreviations are defined as follows: KS, Kolmogorov-Smirnov; SG, simply gridded; MLS, Microwave Limb Sounder; ISN, isentropic; 3-D, three-dimensional; AM, asynoptically mapped; and RC, reconstructed.

ground-based profiles when calculated only over the lower stratosphere results from an increase in the individual correlation coefficients for ~60%–70% of the profiles, with the largest fraction increasing for the 3-D calculations initialized with SG data (19 out of 28 profiles showed an increase in the correlation coefficient). Very small increases in the correlation coefficients for calculated over MLS observed Δ3P profiles are seen for 3-D runs in the middle stratosphere initialized with SG and RC data; the individual correlation coefficients increased in the middle stratosphere for 67%, 55%,

and 50% of the profiles for 3-D SG, AM, and RC initializations, respectively.

The average rms differences for all categories in Table 1 increase for calculated profiles. These results present at first glance an unimpressive record for the calculated profiles. However, as discussed by *Fairlie et al.* [1997], these measures are extremely sensitive to the exact position of features in the profiles. Many cases were found where if the calculated Δ3P profiles were shifted with respect to the observed Δ3P profiles by between 0.3 and 2.5 km, the correlation coefficients increased and rms differences decreased dramatically. In the lower stratosphere, ~80% of the calculated Δ3P SG and AM profiles and ~60% of the calculated Δ3P RC profiles show a sufficient increase in the correlation coefficient that the resulting correlation coefficient is significant at the 95% c.l., with most of the shifts being between ~0.3 and 1.5 km. Many factors, including uncertainties in the altitudes of observations and wind fields used for the transport calculations, and uncertainties in diabatic descent, could lead to such offsets.

The KS significance [e.g., *Gibbons*, 1985] gives a measure of agreement in structure independent of possible positional offsets [e.g., *Fairlie et al.*, 1997]. That there is very little increase in KS significance for the raw profiles in the averages shown in Table 1 when comparing calculated and ground-based profiles versus MLS and ground-based profiles further demonstrates that the calculations do not alleviate overall large-scale biases. However, for the Δ3P profiles, the average KS significance improves for all calculation types. While these improvements are small and the standard deviations large, they represent an improvement in ~80%–100% of the profiles (Table 1). The results suggest, also, that 3-D trajectory calculations provide a slight improvement over isentropic calculations in comparisons extending through the middle stratosphere, where diabatic descent rates are larger and are expected to have a noticeable impact on transport over a period of 11–12 days. The KS significances for Δ3P profiles in Table 1 also suggest that the SG and AM initializations do better than the RC initialization at all levels.

KS significance for individual profiles exceeds 0.95 (that is, 95% confidence that the observed and calculated cumulative frequency distributions are the same) for only a few of the cases studied. However, the KS significance for the Δ3P profiles frequently exceeds the expected KS significance (Table 1) by more than one standard deviation. In these cases the KS significance is more than one standard deviation higher than would be expected between the observed profile and a profile that is identical to the observed profile plus a randomly distributed 10% rms error. Where such a result is accompanied by a substantial increase in the KS significance and by the appearance of features that visibly resemble those in the ground-based observations, it seems reasonable to conclude that the calculations do, in fact, show skill in producing small-scale structure resembling that in the observed profiles.

The average results from the statistical comparisons thus show the calculations to have a modest degree of skill in producing small-scale structure like that in the observations, while they do nothing to decrease overall biases. Focusing only on statistical results, however, does not give a complete picture of the phenomenon of ozone lamination. The statistical agreement over an extended vertical range tells us little about whether a calculated profile may include a feature strongly resembling an individual observed lamina, and it is the study of such individual features that may provide insight into how ozone laminae form. In the following we show several examples of individual profiles chosen to highlight cases where individual features resembling those in the ground-based observations appear in the calculated profiles.

3.2. Examples of Observed and Calculated Ozone Profiles

Figure 1 shows a lidar profile observed on the night of March 9–10, 1993, along with profiles from SG, AM, and

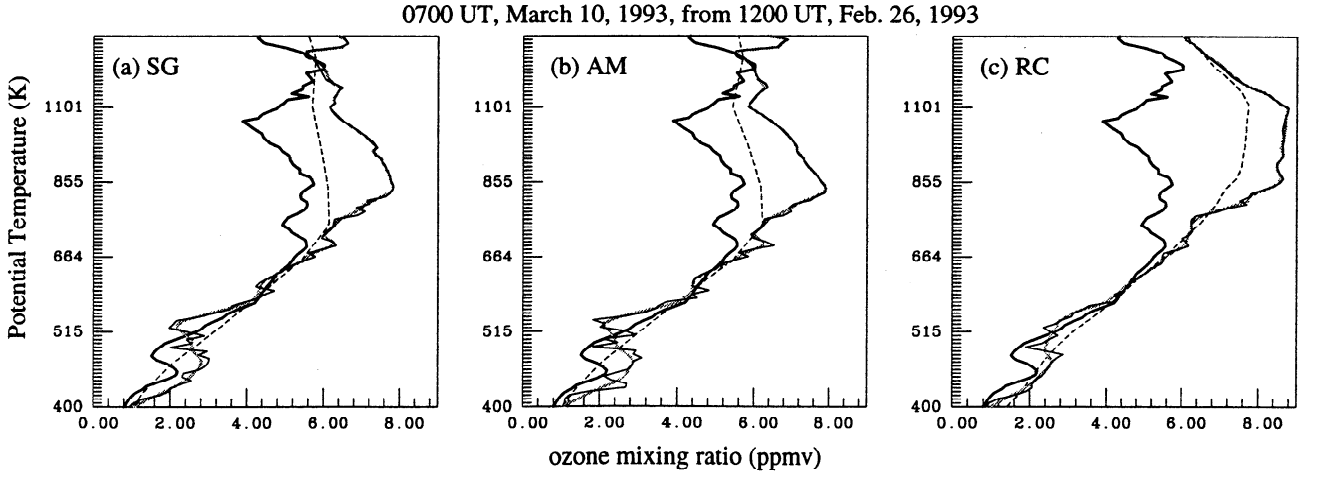

Figure 1. Ozone mixing ratios (ppmv) at the Arctic Stratospheric Observatory (AStrO) on March 10, 1993, from lidar (thick solid black line), Microwave Limb Sounder (MLS) observations (dashed line, interpolated linearly between the 1200 UT March 9 and 10 gridded MLS fields), MLS observations advected forward ~12 days from 1200 UT on February 26, 1993, using an isentropic trajectory calculation, the average of 121 parcels at each level (thick shaded line), and the individual central parcel at each level that is centered over AStrO (thin black line): (a) simply gridded (SG) MLS initialization, (b) asynoptically mapped (AM) MLS initialization, and (c) reconstructed (RC, see text) initialization.

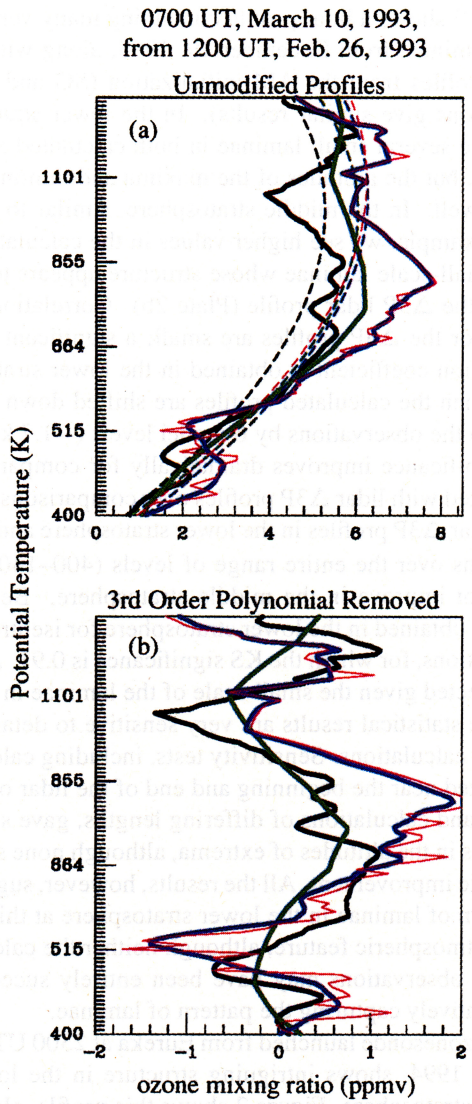

Plate 1. Ozone mixing ratios (ppmv) at AStrO on March 10, 1993, from lidar (thick solid black line), AM MLS observations (thick green line), AM MLS observations advected forward ~12 days from 1200 UT on February 26, 1993, using a three-dimensional (3-D) trajectory calculation (including diabatic descent), the average of 121 parcels at each level (thick blue line), and the individual central parcel at each level that is centered over AStrO (thin magenta line): (a) unmodified profiles, with third-order polynomial fits shown as dashed lines of the corresponding color and (b) profiles with the third-order polynomial fit removed (Δ3P profiles).

RC MLS data, and the high-resolution profiles simulated using isentropic trajectory calculations and the three (SG, AM, and RC) initializations. The lidar profile shows a notch ~2 km deep near 500 K; similar notches appear in each of the calculated profiles, although the calculated notches are positioned higher than that in the lidar profile. Quantitative agreement is poor in the middle stratosphere. Plate 1 shows the lidar and MLS profiles with the profiles resulting from the 3-D trajectory calculation using the AM initialization. Plate 1a shows the raw profiles and third-order polynomial fits to them and Plate 1b shows the Δ3P profiles with these fits removed. Comparing Plate 1a with Figure 1b indicates slightly better (although still not good) agreement between the 3-D calculations and the lidar profile above ~900 K and markedly better agreement above ~1100 K. Examination of maps from isentropic and 3-D calculations at levels above 1100 K indicates that while the patterns of horizontal transport are very similar over this range of levels for both runs, the diabatic descent is sufficiently rapid that much lower ozone from higher levels is advected into the anticyclone (which is over AStrO) near 1200–1400 K in the 3-D calculation.

The correlation coefficient for this case calculated over 400–1400 K for the Δ3P MLS and lidar profiles is significant at the 95% c.l., reflecting the presence of ozone variations on scales large enough that the low-resolution MLS observations capture a smoothed version of them. The correlation coefficient is much lower for the isentropic calculations and slightly lower for the 3-D calculations. In the middle stratosphere this disagreement results mainly from the

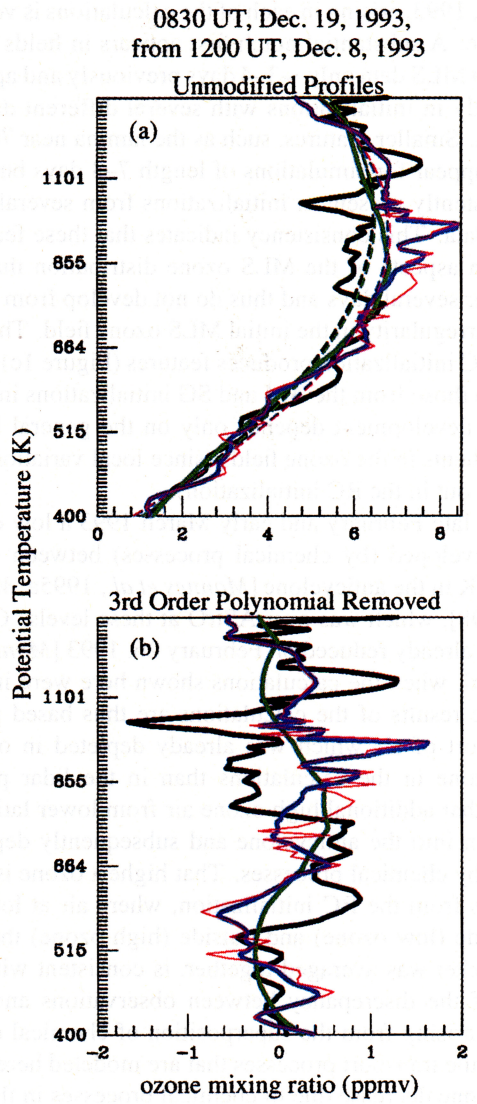

Plate 2. As in Plate 1 but for December 19, 1993, with the calculated profiles advected from December 8, 1993, using a 3-D trajectory calculation.

high calculated values between ~700 and 1100 K, and in the lower stratosphere from the offset in the vertical position of the calculated and observed lamina. When correlation coefficients are calculated for the middle stratosphere only (665–1100 K), the agreement between the Δ3P lidar and calculated profiles improves dramatically (and is much better than between the Δ3P lidar and MLS profiles) because the third-order polynomial fit over those levels removes much of the high bias in the calculations and the smaller-scale laminae agree well. For the lower stratosphere (400–655 K), if the calculated profiles are shifted downward by 4 model levels (~1.2 km) with respect to the lidar profile, the correlation coefficient increases dramatically and is significant at the 95% c.l. The KS significance for the March 10, 1993, Δ3P lidar and calculated profiles is for all calculations greater than for the Δ3P lidar and MLS profiles; for the 3-D middle stratosphere calculations the KS significance level for the average calculated profile is 0.57, well above the expected KS significance (0.23 ± 0.18).

The notch resembling the observed feature near 500 K on March 10, 1993, arising in each of the calculations is very reproducible. A substantial notch first appears in fields simulated from MLS data only ~3–4 days previously and appears consistently in initializations with several different days of MLS data. Smaller features, such as the lamina near 700 K, begin to appear for simulations of length 7–8 days but also are consistently present in initializations from several days of MLS data. This consistency indicates that these features arise from aspects of the MLS ozone distribution that are present for several days and thus do not develop from some transient irregularity in the initial MLS ozone field. The fact that the RC initialization produces features (Figure 1c) comparable to those from the AM and SG initializations implies that their development depends only on the general large-scale gradients in the ozone fields (since local variations are smoothed out in the RC initialization).

During late February and early March 1993 a low ozone pocket developed (by chemical processes) between ~800 and 1200 K in the anticyclone [*Manney et al.*, 1995a; *Morris et al.*, 1998], which was over AStrO at these levels. Ozone there was already reduced on February 26, 1993 [*Manney et al.*, 1995a], when the calculations shown here were initialized. The results of the calculations are thus based partly on transport of air which was already depleted in ozone; higher ozone in the calculations than in the lidar profile suggests that additional high ozone air from lower latitudes was drawn into the anticyclone and subsequently depleted in ozone by chemical processes. That highest ozone is seen in profiles from the RC initialization, where air at low PV from inside (low ozone) and outside (high ozone) the low ozone pocket was averaged together, is consistent with the picture of the discrepancy between observations and calculations arising from the superposition of chemical ozone loss onto the transport processes that are modeled here. The rate of ozone decrease due to chemical processes in this region determined by *Manney et al.* [1995a] and *Morris et al.* [1998] (~$2\%d^{-1}$) is consistent with the magnitude of the bias between calculations and observations.

Plate 2 shows a lidar profile containing many very small-scale laminae, from December 19, 1993, along with calculated profiles from the AM initialization (SG and RC initializations give similar results). In the lower stratosphere there are several small laminae in both calculated and lidar profiles, but the altitudes of the maxima and minima do not match well. In the middle stratosphere, similar to the previous example, we see higher values in the calculations but with small-scale laminae whose structure appears to follow that in the Δ3P lidar profile (Plate 2b). Correlation coefficients for the Δ3P profiles are small; a significant positive correlation coefficient is obtained in the lower stratosphere only when the calculated profiles are shifted down with respect to the observations by 6 model levels (~1.7 km). The KS significance improves dramatically for comparisons of calculated with lidar Δ3P profiles over comparisons of MLS with lidar Δ3P profiles in the lower stratosphere and for calculations over the entire range of levels (400–1400 K) but does not improve in the middle stratosphere. Best agreement is obtained in the lower stratosphere for isentropic AM calculations, for which the KS significance is 0.91. As might be expected given the small scale of the laminae in this profile, the statistical results are very sensitive to details of the various calculations. Sensitivity tests, including calculations initialized near the beginning and end of the lidar observing period and calculations of differing lengths, gave small differences in the altitudes of extrema, although none showed a dramatic improvement. All the results, however, suggest that a pattern of laminae in the lower stratosphere at this time is a real atmospheric feature, although neither the calculations nor the observations may have been entirely successful in quantitatively capturing the pattern of laminae.

An ozonesonde launched from Eureka at 2300 UT on January 1, 1994, shows intriguing structure in the lower and middle stratosphere. Figure 2 shows this profile, along with MLS data and profiles from isentropic calculations. Plate 3 shows the profiles from the 3-D transport calculations and the corresponding fits and Δ3P profiles. All of the calculations produce small laminae below ~440 K and a pair of laminae near 650 K resembling those in the ozonesonde profile. The AM-initialized profile, in addition, produces a series of small laminae between ~450 and 500 K similar in structure to those in the ozonesonde profile. The quantitative resemblance of the notch between 400 and 450 K to that in the ozonesonde profile is strongest for the isentropic calculations (compare Figure 2a with Plate 3a). For calculations over 400–790 K (the range shown in Figure 2 and Plate 3), the correlation coefficients between the calculated Δ3P profiles from the AM initialization and the ozonesonde profile are significant at the 95% c.l. and are much higher than those for the AM MLS profile. The highest KS significances for comparisons with this observed profile are 0.45 (0.76) for the isentropic AM calculations, for average (central) profiles, compared to an expected KS significance of 0.07 ± 0.10 and a KS significance for the MLS profile compared with the ozonesonde profile of 0.05. The correlation coefficients do not improve for the calculations initialized with RC data and KS significance remains low. The above

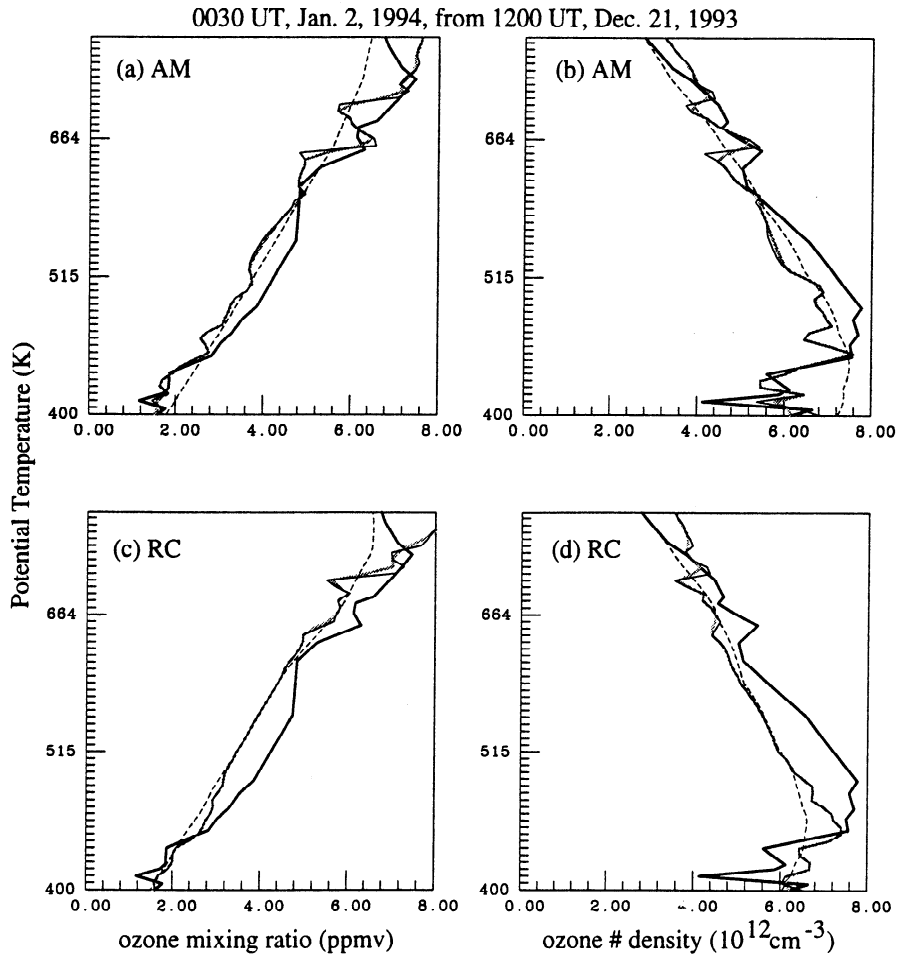

Figure 2. Calculated profiles showing features similar to those in observations from an ozonesonde launched from Eureka. As in Figure 1 but for January 2, 1994, from (a) and (b) AM and (c) and (d) RC MLS data (dashed lines), advected from 1200 UT on December 21, 1993, using an isentropic trajectory calculation, the 121 parcel average (thick shaded line) and the central parcel (thin black line). Figures 2a and 2c show mixing ratio (ppmv); although all calculations are done in terms of mixing ratio, number densities (10^{12} cm^{-3}) are shown in Figures 2b and 2d to emphasize variations in the lower stratosphere (number densities for the calculated and MLS profiles are obtained using UKMO temperatures).

results suggest that some details in the AM initial field that are smoothed out in the RC initial field are important to producing structure similar to that in the ozonesonde observations at these levels.

Figure 3 shows profiles from lidar observations and calculations for March 13, 1994, from 3-D SG and RC calculations. The lidar profile on this night was taken over a shorter than usual time period, and the lidar observations above ~900 K have uncertainties larger than the observed ozone values. The laminar structure with a peak near 490 K and minimum near 470 K is not apparent in the RC-initialized profile. Plate 4 shows the Δ3P lidar profiles with those from the SG and RC calculations. Comparing Plate 4a with Plate 4b indicates that while the RC calculation does not produce a feature resembling the lamina near 470–490 K, it does produce a lamina near 800 K, although this does not as strongly resemble the lamina at that level in the lidar profile as does the one in the SG calculation (Plate 4a). For the AM and SG initializations the correlation coefficients between the calculated and lidar observed Δ3P profiles increase dramatically over those between the MLS and lidar Δ3P profiles. For comparisons over 400-655 K the KS significances are 0.76 (0.91) and 0.99 (0.99) for average and central profiles with SG (AM) initializations; for the RC-initialized profiles the corresponding KS values are ~0.003. The KS significance for the central AM and SG profiles indicates a 99% probability that the cumulative frequency distributions are the same.

Finally, in Figure 4 we show profiles from an ozonesonde launched from Eureka at 2300 UT on March 2, 1996, with simulated profiles from 3-D calculations initialized with SG and RC MLS data (AM MLS data are not available for this period). A feature resembling the observed abrupt ozone increase near 600 K is apparent in both SG and RC calculated profiles and closely matches the feature in the ozonesonde profile. A feature resembling the observed peak near 460 K is present in the SG-initialized calculation, albeit at a lower altitude, but not in the RC calculation. The KS significance

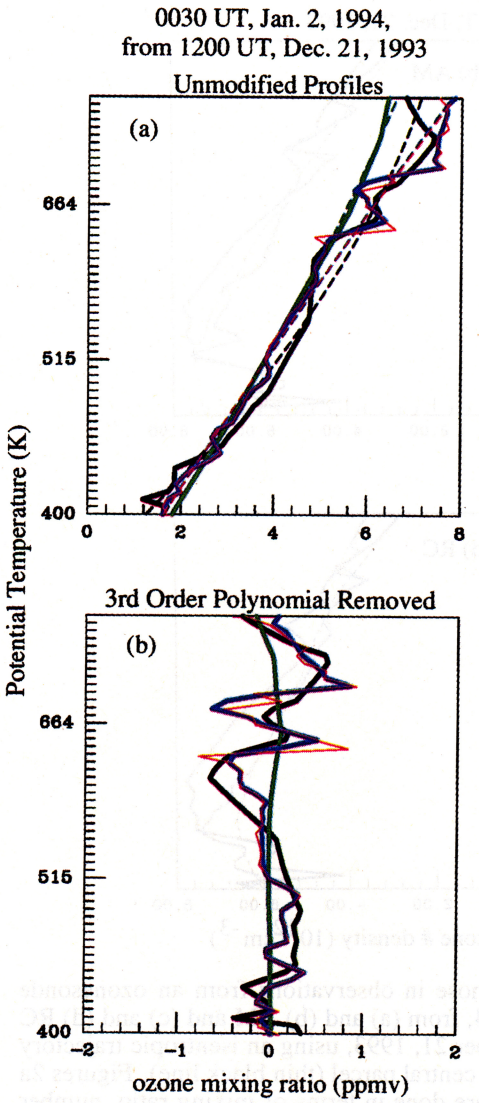

Plate 3. As in Plate 2 but for the January 2, 1994, ozonesonde profile, with the calculated profiles from a 3-D trajectory calculation initialized on December 21, 1993.

levels calculated for the lower stratosphere (400–655 K) are 0.91 (0.98) and 0.75 (0.75) for SG and RC average (central) calculated profiles, respectively, compared to ~0.001 for MLS SG and RC profiles. Thus both calculations show some skill at producing small-scale features resembling the ozonesonde observations, with the production of a feature resembling the lamina near 460 K by the SG run reflected in higher KS values for that profile.

The exact position and shape of the calculated lamina near 460 K changes somewhat depending on the day of MLS data used for initialization, indicating sensitivity to MLS measurement errors or uncertainties due to the MLS sampling pattern and gridding. Note that the calculated profiles for March 3, 1996, have consistently higher ozone mixing ratios than those observed in the lower stratosphere. Ozone depletion during this period in 1996 was the most rapid yet observed in the Arctic [*Manney et al.*, 1996], and *Donovan et al.* [1996] used lidar observations from AStrO during this period to show that chemical depletion was occurring during late February and early March 1996. The chemical depletion was sufficiently rapid at this time that a noticeable change would be expected over the 11–12 days of the run shown here.

In each example above, calculations produced structure resembling one or more features in the ground-based observations. We now examine in detail how these features arise.

3.3. Origins of Laminae

3.3.1. Lamination through filamentation and vortex-edge crossing. It has previously been shown [e.g., *Orsolini*, 1995] that filamentation can lead to lamination in tracer profiles as vertically tilted filament sheets pass over a measurement location. Several laminae in the examples shown above arise in this manner. Plate 5 shows maps from reverse-trajectory calculations for March 10, 1993, near the

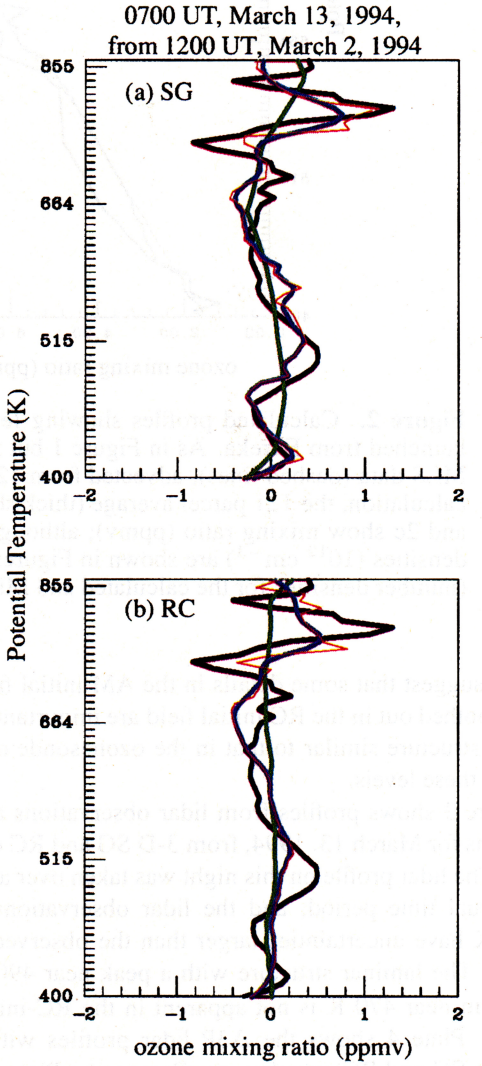

Plate 4. Profiles for March 13, 1994, with third-order polynomial fit from 400 to 865 K removed for (a) SG and (b) RC MLS data and initializations. The heavy black line shows lidar profile; the green line shows MLS data; the blue line shows the calculated profile from the average of 121 points at each level, and the thin magenta line shows the calculated profile from the individual parcels centered over AStrO.

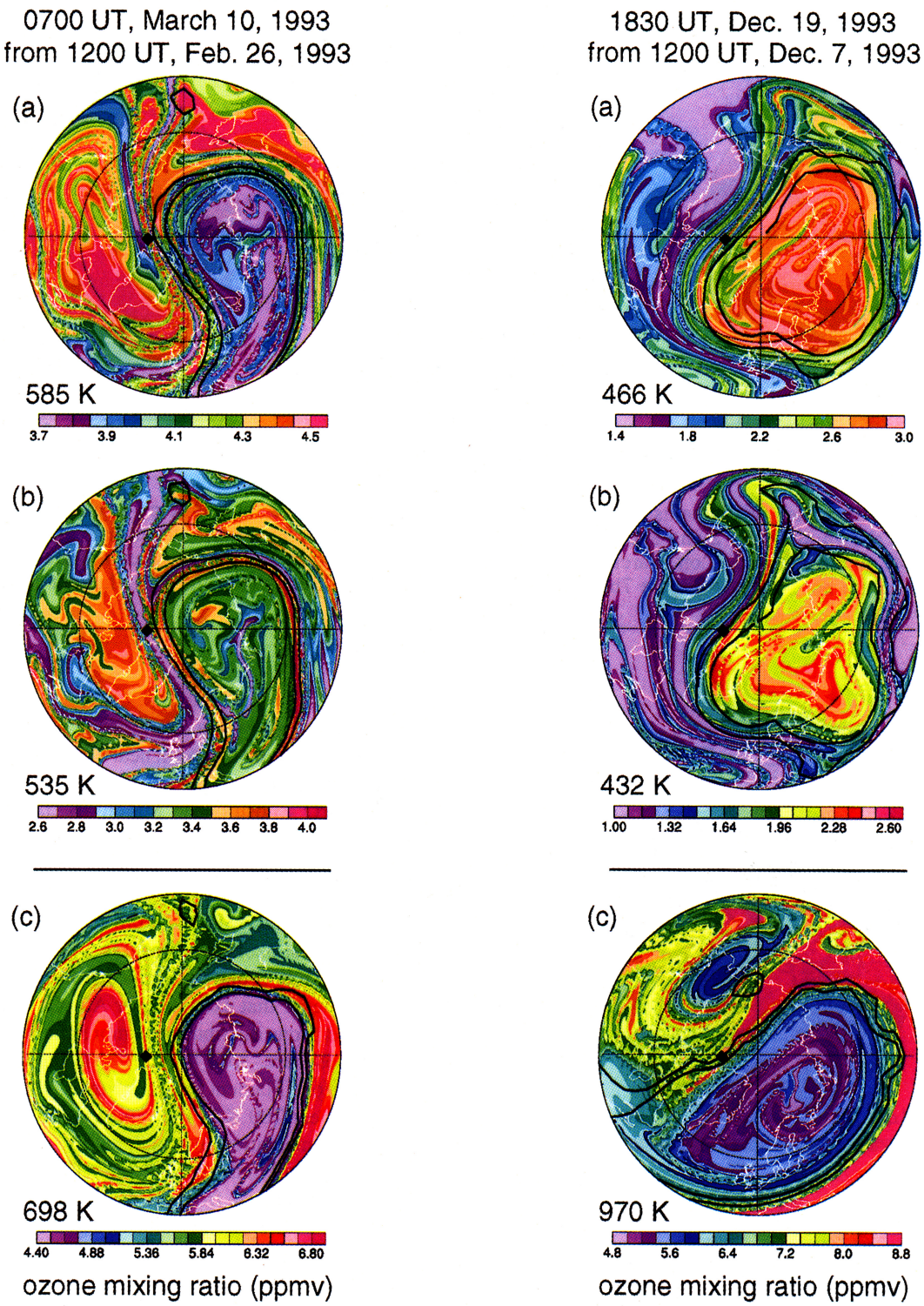

Plate 5. Maps of ozone mixing ratio (ppmv) on March 10, 1993, from AM MLS ozone advected forward isentropically from 1200 UT on February 26, 1993, showing origins of laminae in profiles shown in Figure 1 and Plate 1. The projection is orthographic, from 40° to 90°N, with 0° longitude at the bottom of the plot and the dashed circle showing 60°N. The location of AStrO is given by the black diamond. Maps are for (a) 585 K, (b) 535 K, and (c) 698 K; these θ values are selected from the set of 100 levels at which the profile calculations were run. Note that the color scales are different at different levels to emphasize the ozone gradients at each level. Overlaid black contours are two potential vorticity (PV) contours in the region of strong PV gradients along the vortex edge. Maps are produced from trajectory calculations done on an ~50 km by 50 km equal-area grid with the resultant fields interpolated linearly to a 0.5° latitude by 1.8° longitude grid for plotting.

Plate 6. Filaments corresponding to maxima and minima in the ozone profile shown in Plate 2. As in Plate 5 but for December 19, 1993, advected from December 7, 1993, at (a) 466 K, (b) 432 K, and (c) 970 K.

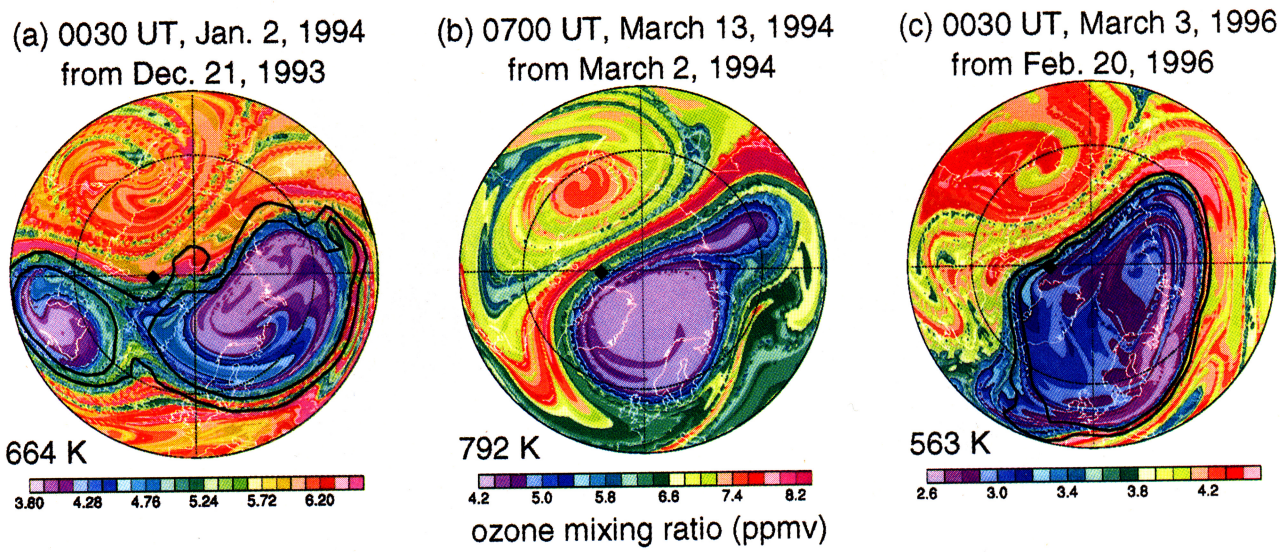

Plate 7. Examples of filaments resulting from vortex-edge crossing: (a) at 664 K on January 2, 1994 (profile shown in Figure 2 and Plate 3), (b) at 792 K on March 13, 1994 (profile shown in Figure 3 and Plate 4), and (c) at 565 K on March 3, 1996 (profile shown in Figure 5). Layout is as in Plate 5. PV contours are not shown in Figure 7b since the outer contour lies directly over the thin filament of high ozone.

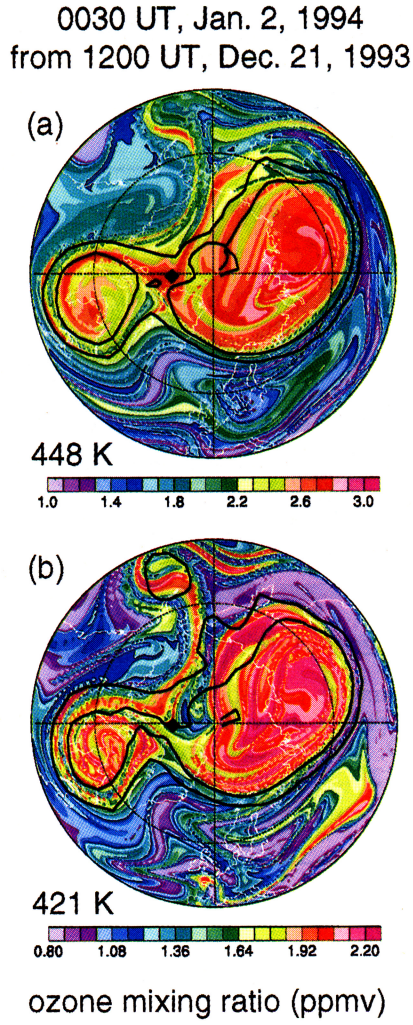

minimum of and above the notch in the lower stratosphere and near the maximum of a peak near 700 K in the calculated profile shown in Figure 1 and Plate 1a. In the lower stratosphere, AStrO's position on March 10, 1993, was along the vortex edge and air from low latitudes was being drawn up around the vortex. The vortex tilted westward and equatorward with height, away from AStrO. Near 460 K (not shown) the air over AStrO is from along the vortex edge where the highest ozone was observed. The extremely low ozone near 535 K (Plate 5b) comes from a large filament of low-latitude air that extends over AStrO, while at 585 K (Plate 5a) the ozone distribution is more characteristic of the middle stratosphere, with higher ozone outside the vortex and a high-ozone filament extending over AStrO.

A lamina near 700 K in the same profile (Plate 5c) also arises from filamentation, although in this case it is not along the vortex edge but in the anticyclone. The variations in the calculated laminae arise from the positioning of filaments of high and low ozone that are coiled together in the anticyclone over AStrO, for example, the high ozone filament that passes over AStrO in Plate 5c. This peak in the calculations corresponds to a peak in the lidar observations. The feature in the lidar profile probably arises from the superposition of this filamentation on the rapid chemical ozone decrease that is known to be occurring in the anticyclone at this time [*Manney et al.*, 1995a; *Morris et al.*, 1998].

Plate 8. Illustration of a lamina resulting from an intrusion into the vortex. Maps are for January 2, 1994, from isentropic calculations initialized with AM MLS data on December 21, 1993, at (a) 448 K and (b) 421 K. Layout is as in Plate 5.

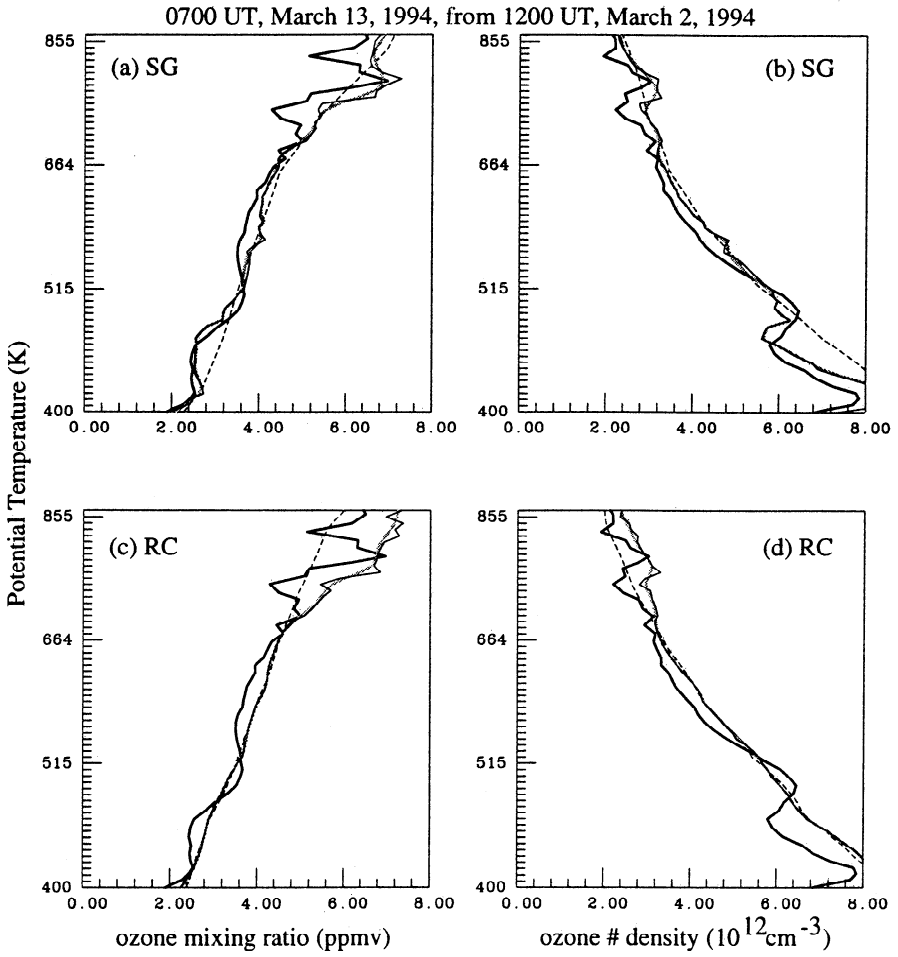

Figure 3. As in Figure 2 but for a lidar profile and SG and RC MLS ozone, for March 13, 1994, with calculated profiles from a 3-D trajectory calculation initialized on March 2, 1994. The lidar observation period on this night was shorter than usual; hence, above ~900 K, uncertainties in the lidar profile are sufficiently large that useful information is not obtained; these levels are not shown.

Lamination in the calculated profiles for December 19, 1993 (shown in Plate 2), also arises from filamentation. In this case the calculations show reproducible minima near 430 and 500 K, with a maximum between. Plate 6 shows that this pattern arises from the positioning over AStrO of narrow interwoven filaments of high ozone pulled off the vortex edge and low ozone drawn up from low latitudes. The maximum near 466 K results from a filament of high-ozone air that is pulled off the vortex edge (Plate 6a) while the minimum below it indicates a filament of low-ozone air pulled up around the vortex edge from low latitudes (Plate 6b); the maximum near 500 K results from a similar high-ozone filament (not shown). The lidar profile showed a similar pattern (Plate 2) but with the extrema at different altitudes. Note that these filaments are much narrower than the ones that produced the deep notch in the lower stratosphere on March 10, 1993. For such narrow filaments the altitude of the modeled laminae will be more sensitive to uncertainties in the exact horizontal position of the filaments or the exact time at which they are at a given position (because of uncertainties in the winds used in the transport calculations).

The calculated profiles for December 19, 1993 (Plate 2), also show a minimum near 1007 K and a maximum near 970 K that are reminiscent of features in the lidar profile, although the mixing ratios are ~0.5 ppmv higher in the calculations. These features are near the vortex edge, in the region between the vortex and the anticyclone. As in the previous example, an extensive low ozone pocket had formed in the anticyclone [*Manney et al.,* 1995a]. The maximum near 970 K resulted from air drawn up from low latitudes passing over AStrO before being entrained into the anticyclone (Plate 6c). The rapid chemical processes responsible for creating the low ozone pocket begin depleting the air of ozone as it moves to high latitudes, even before it is entrained into the anticyclone [*Morris et al.,* 1998], which may contribute to the higher values seen in the calculated profiles (since no chemical processes are represented there). Also, MLS tropical ozone observations in the middle stratosphere (where the air forming this lamina originates) have been shown to have a small high bias with respect to correlative data [*Froidevaux et al.,* 1996].

In Plate 7 we show three examples of lamination along the

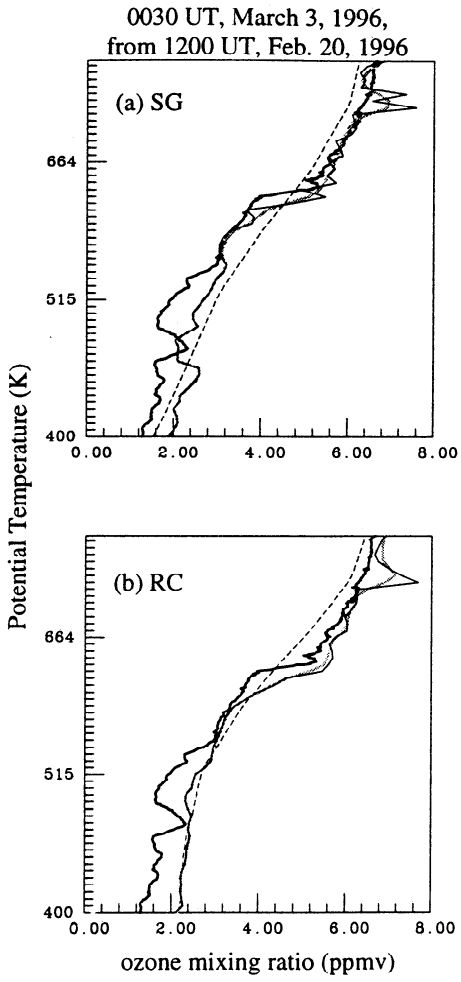

Figure 4. As in Figure 3 but showing mixing ratio only for March 3, 1996, with calculated profiles from a 3-D trajectory calculation initialized on February 20, 1996.

vortex edge. In each case, material with high ozone had been drawn up around the vortex edge so that at one level, high ozone typical of low latitudes was over the location of the ground-based observations and a few levels away, low ozone characteristic of the vortex was over the same location. The pair of laminae with a peak near 660 K on January 2, 1994 (Figure 2), developed during a strong stratospheric warming, when large tongues of high ozone had been both entrained into the strong anticyclone and advected around the polar vortex. At 664 K a large tongue of high ozone that has been advected around the vortex is directly over Eureka (Plate 7a), while slightly lower (at 640 K), this tongue is positioned slightly to the west, with air much lower in ozone characteristic of the vortex over Eureka. The calculated lamina near 800 K on March 13, 1994 (Figure 3 and Plate 4), originated in a similar manner, but in this case a rather narrow filament of relatively high ozone air was wrapped around the vortex and at 800 K was directly over AStrO. On March 3, 1996, at 563 K the inner edge of the vortex (with very low ozone) was just over Eureka (Plate 7c); a few levels higher, the position of Eureka is not only at the outside of the vortex edge but also in a region where a thick tongue of high ozone extended around the vortex edge. The feature that formed in this case is not strictly a lamina but rather an extremely abrupt ozone increase seen in the calculated and ozonesonde profiles (Figure 4).

These examples of lamination related to filamentation and vortex edge crossing are all cases where the calculated profiles from all types of initialization contained laminae corresponding to features in the lidar or ozonesonde profiles. Since lamination produced this way depends only on the advecting winds and the largest-scale features in the initial ozone field (i.e., the overall latitudinal ozone gradients and the strong ozone gradients between the vortex exterior and interior) that tend to be very well correlated with PV, even the smooth RC initialization fields contain the basic overall structure that is important to their formation.

3.3.2. Lamination through intrusion into the vortex. There are several examples in our calculations where lamination arose in conjunction with intrusions into the vortex. Plate 8 shows one such example in the lower stratosphere on January 2, 1994 (profiles shown in Figure 2). The vortex was relatively weak in the lower stratosphere at this time, and Plate 8b shows that the notch below 450 K results from a tongue of very low ozone intruding deep into the vortex. The vertical extent of this tongue is from 400 K (or below) to ~440 K; above that (e.g., Plate 8a), high ozone characteristic of the vortex is over Eureka. The tongue of low ozone itself is relatively broad but has considerable fine structure within it, so its exact location with respect to Eureka's position results in the smaller-scale variations seen in the calculations in Figure 2, and the magnitude of notches produced in the calculations depends on these details. While the RC initialization produced a small notch in this region with qualitatively similar small-scale structure, the notch produced in calculations with SG and AM initializations was considerably deeper and matched the feature in the ozonesonde profile more closely.

Figure 5 shows a lidar profile observed on December 10, 1993, along with calculated profiles from AM and RC initializations. The AM-calculated profile contains a relatively broad lamina with a maximum near 580 K and a minimum near 620 K which strongly resembles one in the lidar observations, while the RC-calculated profile shows a much smaller minimum. Plate 9 shows that the ozone maximum arises from an intrusion of air into the vortex over AStrO. Although the intrusion extends over many levels (compare Plates 9a and 9b), the details of the lamina produced in the calculations depends on the exact calculated position of this intrusion with respect to AStrO. The differences between the AM- and RC-initialized profiles suggest that some of the finer-scale features (albeit still large enough to be captured by MLS) in the AM field that are smoothed out in the RC field may be important in simulating this feature.

3.3.3. Lamination through advection of local features. It is common to find that ozone in the Arctic lower stratospheric vortex is rather inhomogeneous and not particularly well correlated with PV. This may occur because there is chemical ozone depletion, because there are variations in the patterns of diabatic descent (which affects PV and chemical tracers differently), and/or simply because there are inaccu-

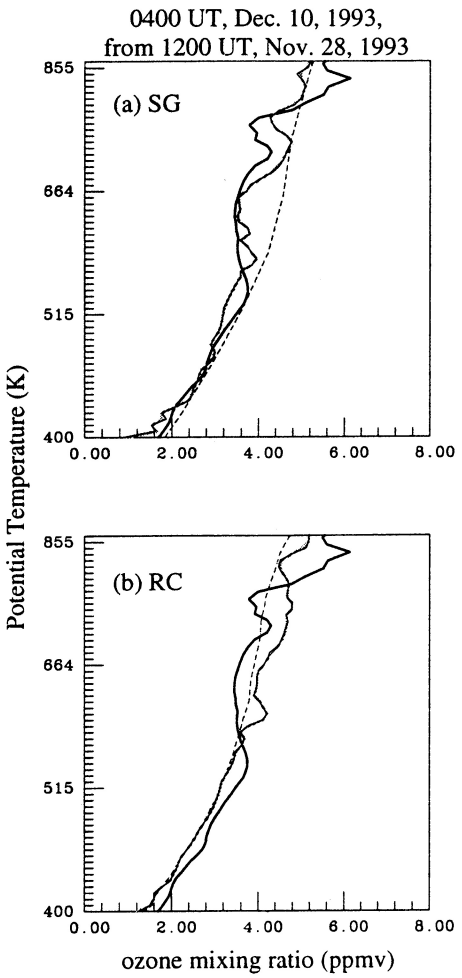

Figure 5. As in Figure 4 but for profiles on December 10, 1993, for lidar observations (thick black line): (a) SG and (b) RC MLS observations (thin dashed line) and calculations initialized on November 28, 1993 (thick shaded line shows average of 121 parcels, and thin black line shows individual parcels centered over AStrO; in this case, these lines are nearly identical).

racies in the calculated PV fields so that they do not capture local features that are present in the real atmosphere. In several of our calculations, ozone laminae developed in the lower stratosphere as a result of such features in the MLS initialization fields.

In Figure 3 and Plate 4 we showed a lidar profile on March 13, 1994, with a strong lamina in the lower stratosphere; the AM- and SG-calculated profiles produced a very similar feature, but no such feature was apparent in the RC calculation. Plate 10 shows the RC and SG initialization fields on March 2, 1994, with the locations of the parcels from the calculated profile at 472 K (the level of the local ozone minimum), and the SG-calculated field on March 13, 1994. The air over AStrO on March 13, 1994, was, 11 days previously, in a localized region of low ozone within the vortex. Although the detailed shape varies slightly, this feature also appears in the AM MLS ozone. Examination of the ungridded MLS data along orbit tracks indicates that this region of low ozone is defined by at least eight MLS observations on at least four orbits, comprising both ascending and descending tracks, confirming that this feature does not result from one or two spurious MLS observations. The RC field is much smoother, with only a slight ozone decrease in this region. Such a region of low ozone in the vortex could result from local chemical loss or local variations in diabatic descent (both of which were occurring during this period [*Manney et al.*, 1995b]) or could be a remnant of a previous intrusion of low-latitude air into the vortex. Whatever its origin, that such a feature must be present in order to produce a profile whose shape follows that of the independently observed profile over AStrO 11 days later indicates that both this feature and the lamina seen in the lidar profile at AStrO are real atmospheric features.

Plate 11 shows the origin of the calculated lamina near 450 K on March 3, 1996 (Figure 4). Below ~600 K the vortex was over Eureka, and the nonuniform distribution of ozone within the vortex results in alternating layers with low (Plate 11a) and high (Plate 11b) ozone over Eureka. As in

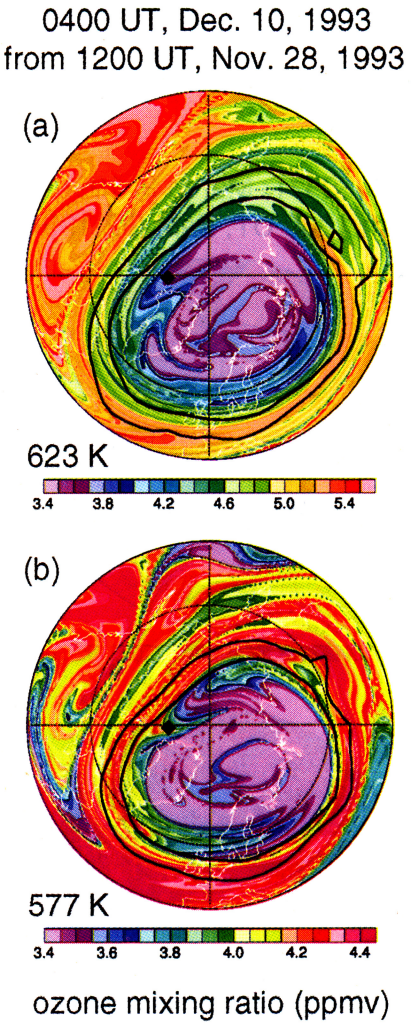

Plate 9. Origins of (a) minimum near 623 K and (b) maximum near 577 K seen in calculated profiles in Figure 5 from an intrusion into the vortex. Maps are for December 10, 1993, advected using isentropic trajectory calculations from November 28, 1993.

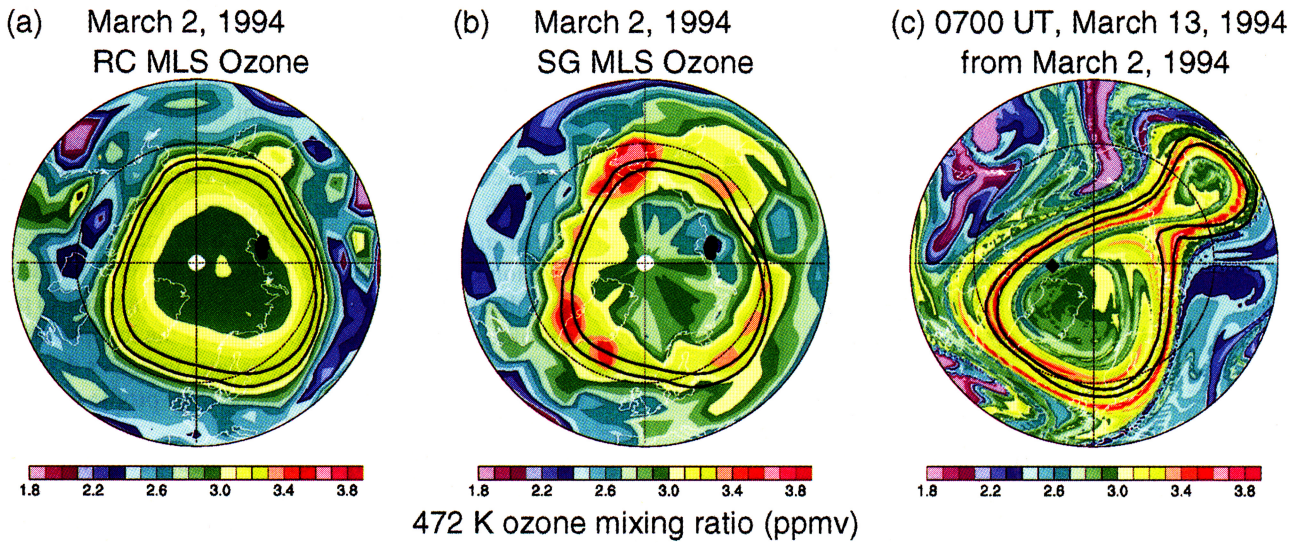

Plate 10. Demonstration of the origin of the notch near 472 K seen in the calculated profiles shown in Figure 3 and Plate 4 on March 13, 1994. Maps show (a) the RC initialization field on March 2, 1994, with the locations of the parcels from the profile calculation at that level overlaid, (b) the SG initialization field on March 2, 1994, with the locations of the parcels overlaid, and (c) the 472 K map for March 13, 1994, resulting from the advection of the SG field shown in Plate 10b.

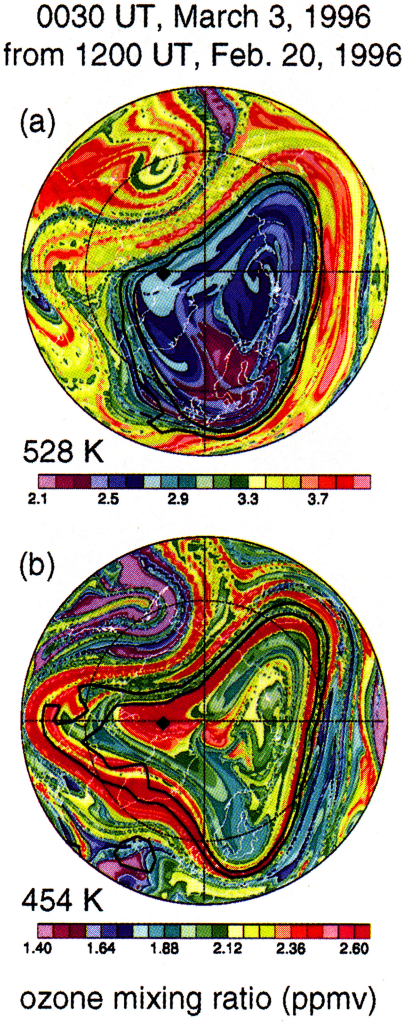

the previous case where the vortex was over Eureka, calculations using RC ozone do not capture this feature, implying that its development is dependent on local variations in the ozone field that are observed by MLS but which are smoothed out in the RC fields. In this case the nonuniform distribution of ozone within the vortex resulted mainly from chemical ozone depletion [*Manney et al.*, 1996].

4. Summary and Conclusions

Coarse-resolution satellite observations of ozone from the UARS MLS were used to initialize reverse-trajectory calculations, producing simulated high-resolution ozone profiles at the location of the AStrO facility near Eureka, Canada. Comparison with many lidar and ozonesonde observations taken at AStrO provides information both on the origins of laminae seen in the ground-based observations and on the consistency between MLS ozone and ozone from the ground-based observations.

Statistical measures of the average agreement between calculated profiles and those from ground-based observations indicate that the calculations do not tend to diminish large-scale biases already present between MLS and ground-based observations. However, when the largest-scale variations are removed, the calculations show a small average

Plate 11. Origin of lamina near 460 K seen in Figure 5 resulting from advection of inhomogeneities inside the lower stratospheric vortex, on March 3, 1996. Maps are for March 3, 1996, initialized with SG MLS ozone on February 20, 1996, at (a) 528 K and (b) 454 K.

improvement in the agreement between small-scale structure over the vertical extent of the profiles or significant sections thereof. The largest (although still modest) and most consistent improvements are seen in the lower stratosphere (~400–650 K). In this region, improvements are seen in the agreement between the frequency distributions for nearly all calculated profiles initialized with gridded MLS data and ~80% of those initialized with the PV/θ-space reconstruction of MLS data. While improvements were seen in only ~50%–65% of the correlation coefficients, and most of these were not statistically significant, dramatic improvements leading to statistically significant correlations were seen in ~80% of the profiles from gridded MLS initializations when a shift of ~0.3–2.5 km is allowed in the altitudes of the profiles. The average results for the entire vertical range studied (400–1400 K) and for the middle stratosphere (~660-1100 K) show smaller improvements, but the results do indicate that for altitudes above ~660 K the 3-D calculations result in closer agreement between the calculated and observed profiles than do the isentropic calculations. This is as expected since above this level, diabatic effects may be significant over the 8–12 day calculation periods used.

We have shown several representative examples of comparisons between individual lidar and ozonesonde profiles and calculated profiles. A few of these show very good quantitative agreement between the ground-based observations and the calculated profiles at levels up to ~850 K, with dramatic improvements in statistical measures of agreement with the ground-based profiles of the calculated profiles over those from MLS data. Other cases do not show such good overall agreement between the calculated profiles and ground-based observations over an extended altitude range, but the calculated profiles contain one or more individual features that strongly resemble features in the ground-based observations.

While all of the small-scale structure in our calculations ultimately arises from differential advection of ozone by the large-scale wind field, examination of the origins of individual features shows three distinct ways in which laminae are produced. First, they may result from filamentation which may or may not be accompanied by the crossing of the vortex edge. Since filamentation results from air being drawn up around the vortex or into the anticyclone from low latitudes and/or air being pulled off the vortex, the formation of laminae in this manner depends only on the very large scale horizontal gradients in the ozone field, which are generally well correlated with PV. Consistent with this, we found that calculations initialized with the highly smoothed PV/θ-space reconstructions (RC fields) produced features comparable to those in the calculations initialized with gridded MLS data when laminae arose by this means. Second, laminae appeared in conjunction with intrusions into the vortex. In these cases, while the calculations initialized with RC fields produced laminae, the agreement between calculated features and those seen in the ground-based profiles was distinctly better for calculations initialized with gridded MLS data, indicating some dependence on the details of the initialization fields. Finally, we have shown examples inside the lower stratospheric vortex where laminae arose from the advection of local features in the MLS initialization fields. In these cases the RC-initialized calculations fail to produce any significant structure.

Laminae formed via the first two processes were seen in both the middle and lower stratosphere. In the middle stratosphere (~650–1100 K) some calculations show poor quantitative agreement but include small vertical scale features mimicking those seen in the ground-based observations. We have shown examples where the magnitude of such biases appears to be consistent with the rate of ozone decrease due to specific chemical processes that are known to be occurring. Above ~1200 K, only calculations including diabatic descent capture the main features of the ozone profiles; increasingly short chemical timescales at these levels may also contribute to poor agreement here between observed and calculated profiles.

Laminae that formed by advection of local features were seen only in the lower stratosphere. *Bird et al.* [1997] showed that laminae well within the lower stratospheric vortex were common, and we have seen behavior similar to the examples shown in many other profiles. This provides further evidence that the distribution of ozone within the Arctic lower stratosphere vortex is typically very inhomogeneous. That local features observed by MLS in these cases are necessary in order to reproduce laminae in independent ground-based observations at AStrO strongly suggests that both represent real atmospheric features.

Acknowledgments. We thank the Staff at the Eureka Weather Station and the MLS team for their support, R. Swinbank and A. O'Neill of the UKMO for meteorological data, O. Uchino and the Science and Technology Agency of Japan for support of ozonesonde measurements, and T. D. A. Fairlie, L. Froidevaux, R. B. Pierce, M. L. Santee, J. W. Waters, and R. W. Zurek for helpful comments. Work at the Jet Propulsion Laboratory, California Institute of Technology, was done under contract with the National Aeronautics and Space Administration. Financial and technical support for CRESTech personnel were provided by the Center for Research in Earth and Space Technology and by the Atmospheric Environment Service of Canada.

References

Appenzeller, C., and J. R. Holton, Tracer lamination in the stratosphere: A global climatology, *J. Geophys. Res., 102,* 13,555-13,569, 1997.

Bird, J. C., S. R. Pal, A. I. Carswell, D. P. Donovan, G. L. Manney, J. M. Harris, and O. Uchino, Observations of ozone structures in the polar vortex, *J. Geophys. Res., 102,* 10,785-10,800, 1997.

Brasseur, G., and S. Solomon, *Aeronomy of the Middle Atmosphere,* 2nd Ed., 441 pp., D. Reidel, Norwell, Mass., 1986.

Carswell, A. I., S. R. Pal, W. Steinbrecht, J. A. Whiteway, A. Ulitsky, and T. Y. Wang, Lidar measurements of the middle atmosphere, *Can. J. Phys., 69,* 1076-1086, 1991.

Donovan, D. P., J. C. Bird, J. A. Whiteway, T. J. Duck, S. R. Pal, and A. I. Carswell, Lidar observations of stratospheric ozone and aerosol above the Canadian High Arctic during the 1994-1995 winter, *Geophys. Res. Lett., 22,* 3489-3492, 1995.

Donovan, D. P., J. C. Bird, J. A. Whiteway, T. J. Duck, S. R. Pal, A. I. Carswell, J. W. Sandilands, and J. W. Kaminski, Ozone and aerosol observed by lidar in the Canadian Arctic during the winter of 1995-1996, *Geophys. Res. Lett., 23,* 3317-3320, 1996.

Elson, L. S., and L. Froidevaux, The use of Fourier transforms for asynoptic mapping: Early results from the Upper Atmosphere Research Satellite Microwave Limb Sounder, *J. Geophys. Res., 98,* 23,039-23,049, 1993.

Fairlie, T. D. A., R. B. Pierce, W. L. Grose, and G. Lingenfelser, Lagrangian forecasting during ASHOE/MAESA: Analysis of predictive skill for analyzed and reverse-domain-filled potential vorticity, *J. Geophys. Res., 102,* 13,169-13,182, 1997.

Froidevaux, L., et al., Validation of UARS MLS Ozone Measurements, *J. Geophys. Res., 101,* 10,017-10,060, 1996.

Gibbons, J. D., *Nonparametric Methods for Quantitative Analysis,* 2nd Ed., Am. Sci., New York, 1985.

Manney, G. L., R. W. Zurek, A. O'Neill, and R. Swinbank, On the motion of air through the stratospheric polar vortex, *J. Atmos. Sci., 51,* 2973-2994, 1994.

Manney, G. L., L. Froidevaux, J. W. Waters, J. C. Gille, R. W. Zurek, J. B. Kumer, J. L. Mergenthaler, A. E. Roche, A. O'Neill, and R. Swinbank, Formation of low ozone pockets in the middle stratospheric anticyclone during winter, *J. Geophys. Res., 100,* 13,939-13,950, 1995a.

Manney, G. L., R. W. Zurek, L. Froidevaux, and J. W. Waters, Evidence for Arctic ozone depletion in late February and early March 1994, *Geophys. Res. Lett., 22,* 2941-2944, 1995b.

Manney, G. L., M. L. Santee, L. Froidevaux, J. W. Waters, and R. W. Zurek, Polar vortex conditions during the 1995-1996 Arctic winter: Meteorology and MLS ozone, *Geophys. Res. Lett., 23,* 3203-3206, 1996.

McDermid, I. S., et al., Comparison of ozone profiles from ground-based lidar, electrochemical concentration cell balloon sonde, ROCOZ-A rocket ozonesonde and stratospheric aerosol and gas experiment satellite measurements, *J. Geophys. Res., 95,* 10,037-10,042, 1990.

Morris, G. A., S. R. Kawa, A. R. Douglass, M. R. Schoeberl, L. Froidevaux, and J. W. Waters, Low ozone pockets explained, *J. Geophys. Res., 103,* 3599-3610, 1998.

Newman, P. A., and M. R. Schoeberl, A reinterpretation of the data from the NASA stratosphere-troposphere exchange project, *Geophys. Res. Lett., 22,* 2501-2504, 1995.

Orsolini, Y. J., On the formation of ozone laminae at the edge of the Arctic polar vortex, *Q. J. R. Meteorol. Soc., 121,* 1923-1941, 1995.

Orsolini, Y., G. Hansen, U. Hoppe, G. Manney, and K. Fricke, Dynamical modelling of wintertime Lidar observations in the Arctic: Ozone laminae, and ozone depletion, *Q. J. R. Meteorol. Soc., 123,* 785-800, 1997.

Pierce, R. B., and T. D. A. Fairlie, Chaotic advection in the stratosphere: Implications for the dispersal of chemically-perturbed air from the polar vortex, *J. Geophys. Res., 98,* 18,589-18,595, 1993.

Pierce, R. B., J.-U. Grooss, W. L. Grose, J. M. Russell, P. J. Crutzen, T. D. Fairlie, and G. Lingenfelser, Photochemical calculations along airmass trajectories during ASHOE/MAESA, *J. Geophys. Res., 102,* 13,153-13,167, 1997.

Plumb, R. A., D. W. Waugh, R. J. Atkinson, P. A. Newman, L. R. Lait, M. R. Schoeberl, E. V. Browell, A. J. Simmons, and M. Loewenstein, Intrusions into the lower stratospheric Arctic vortex during the winter of 1991-1992, *J. Geophys. Res., 99,* 1089-1105, 1994.

Reber, C. A., The Upper Atmosphere Research Satellite (UARS), *Geophys. Res. Lett., 20,* 1215-1218, 1993.

Reid, S. J., and G. Vaughan, Lamination in ozone profiles in the lower stratosphere, *Q. J. R. Meteorol. Soc., 117,* 825-844, 1991.

Santee, M. L., G. L. Manney, W. G. Read, L. Froidevaux, and J. W. Waters, Polar vortex conditions during the 1995-1996 Arctic winter: MLS ClO and HNO_3, *Geophys. Res. Lett., 23,* 3207-3210, 1996.

Schoeberl, M. R., and P. A. Newman, A multiple-level trajectory analysis of vortex filaments, *J. Geophys. Res., 100,* 25,801-25,815, 1995.

Schoeberl, M. R., et al., Reconstruction of the constituent distribution and trends in the Antarctic polar vortex from ER-2 flight observations, *J. Geophys. Res., 94,* 16,815-16,845, 1989.

Steinbrecht, W., *Lidar Measurements of Ozone, Aerosol and Temperature in the Stratosphere,* Ph.D. thesis, York Univ., Toronto, Ont., Canada, 1994.

Steinbrecht, W. and A. I. Carswell, Evaluation of the effects of Mount-Pinatubo aerosol on differential absorption lidar measurements of stratospheric ozone, *J. Geophys. Res., 100,* 1215-1233, 1995.

Sutton, R. T., H. MacLean, R. Swinbank, A. O'Neill, and F. W. Taylor, High-resolution stratospheric tracer fields estimated from satellite observations using Lagrangian trajectory calculations, *J. Atmos. Sci., 51,* 2995-3005, 1994.

Swinbank, R., and A. O'Neill, A stratosphere-troposphere data assimilation system, *Mon. Weather Rev., 122,* 686-702, 1994.

Waugh, D. W., et al., Transport out of the lower stratospheric Arctic vortex by Rossby wave breaking, *J. Geophys. Res., 99,* 1071-1088, 1994.

J. C. Bird, A. I. Carswell, D. P. Donovan, and S. R. Pal, Lidar Laboratory, Center for Research in Earth and Space Technology, 4850 Keele St., North York, Ontario, Canada, M3J 3K1.

T. J. Duck, Department of Physics and Astronomy, York University, 4850 Keele St., North York, Ontario, Canada, M3J 3K1.

G. L. Manney, Mail Stop 183-701, Jet Propulsion Laboratory, Pasadena, CA 91109. (e-mail: manney@mls.jpl.nasa.gov)

J. A. Whiteway, Department of Physics, University of Wales, Aberystwyth, Wales, SY23 3BZ, U.K.

(Received March 3, 1997; revised November 12, 1997; accepted November 25, 1997.)